Nigerian Journal of Mathematics and Applications
Volume 32 (II); (2022); 14 41: Printed by Unilorin press
© Nig: J: Math: Appl: http : ==www:njmaman:com

Special Issue in Honor of Prof. J. A. Gbadeyan's Retirement

Dynamics of Non-Newtonian Nano uid Flow Past a Semi-In nite Vertical Porous Plate Under the In uence of Lorentz Force and Soret-Dufour Mechanism

Ahmed Lukman Olalekan

Abstract

This paper considered the boundary layer behavior, and e ects of magnetohydrodynamic (MHD) and viscous dissipation on the simultaneous ow of Casson and Walter-B viscoelastic nano uid past a vertical penetrable plate in the presence of heat generation, radiation, chemical reaction, Soret, and Dufour mechanism. The nature of Casson uids examined in the study are blood and uid juice. These two non-Newtonian uids are made to ow into the layer over the vertical plate with the nanoparticles located in the hot region at the layers. The set of governing partial di erential equations (PDE) that represents the model were simpli ed to non-dimensional quantities, decoupled via Gauss-Seidel approach, and then solved numerically employing spectral relaxation method (SRM). The investigation revealed that, the imposed thermal radiation along with heat generation greatly a ects the uid temperature, and thermal layer due to the hotness within the boundary layers, while the applied magnetic eld degenerates the uid velocity.

1. Introduction

The problem of non-Newtonian boundary layer liquids ows is the connection between shear stress together with the proportion of shear strain. Non-Newtonian liquids such as Casson, and micropolar, generally exhibit complex characteristics not known with their Newtonian counterparts, and as such, they are explored under deformation and ow in science. Most researchers of recent have devoted their investigations on this type of uids

Received: 11/06/2022, Accepted: 10/07/2022, Revised: 29/07/2022. Corresponding author.
2015 Mathematics Subject Classi cation. 76A05 & 76W05.
Keywords and phrases. Soret-Dufour, Dimensionless equations, Magneto-nano uid, SRM, MHD, Viscous dissipation
Department of Mathematics, Baze University, Abuja, Nigeria
E-mails of the corresponding author: lukman.ahmed@bazeuniversity.edu.ng
ORCID of the corresponding author: 0000-0002-8823-3057

owing to their rheological entreaty in mechanical as well as chemical engineering techniques. The motion of non-Newtonian liquids takes place in avalanches, and mud slides. It has applications in many processes in such industry involving food processing like honey, yogurt, and ketchup; biological materials (blood), chemicals (the polymers), pharmaceutical production of personal care items (shampoo, creams) and many more. The problem of MHD viscoelastic nanofluid flow has been considered by [1]. They used the variational finite element method in solving their flow equations. Their outcome shows that raising Deborah number increases the velocity profile. [2] have studied MHD viscoelastic fluid flow. They considered Soret along with Dufour in their study. They found out that temperature profiles are less sensitive to the large value of the Lewis number. [3] have equally examined chemical reaction impact on MHD motion of viscoelastic liquid. It was finalized in the analysis that the chemical species greatly affect the momentum boundary layer. The recent study of [4] elucidates on the boundary layer problem of steady, laminar along with the flow of MHD viscoelastic fluid. The transformed flow equations were perturbed and the result revealed that elasticity, as well as suction, are ineffective the moment skin friction is large. In the work of [5], flow of Walters-B liquid past an accelerating permeable surface was investigated. Their motion analysis was numerically solved via spectral homotopy analysis method (SHAM). It was concluded in their analysis that, higher viscoelastic term degenerates fluid velocity.

The nanofluid contains nanometer-sized particles and are popularly referred to as nanoparticles. The study of nanofluid can be homogeneous involving two-phase methods. Many science and technological investigations have been explored on the influence of thermal conductivity on nanofluid. The most important aspect of nanofluid is its size, and temperature. The nanofluid has large colloidal suspension stability and it is important in heat transfer along with transport properties when its size, shape, or concentration along particle material is altered. The nanoparticles have both biomedical and environmental applications. The environmental applications finds usefulness in water treatment, bioremediation of diverse contaminants, and in the production of clean energy, while the biomedical applications are basically found in the imaging, biosensor, as well as drug delivery. The study of [6] examined nanoparticle and base fluid types. It is reported from the study that, the heat transport coefficient is highest for water alumina/water nanoliquid particle with higher magnitude of thermal conductivity. [7] have discussed in their work, the impact of nano-particles in bubble absorption and its activeness in a binary fluid. The impact of thermophoresis on nanoparticle distribution has been investigated by [8]. It was found out in the study that the presence of large particles gives non-uniformity in concentration distribution. Also [9] studied Grain's size together with the shape reliance of luminescence efficiency. The method of sedimentation was used and the rod similar grain screens show together with a reduction in efficiency of luminescence values. The recent exploration of [10] presented the heat transport behavior of nanofluids flows in microchannels. It was found out in their study that much viscosity of nanofluids in comparison to water, power pumping which is required in the driving flow of nanofluid in microchannels elevates. [11], further elucidates on the heat transport of nanofluids situated in a microchannel considering heat sink in a V-type inlet/outlet boundary. It was finalized in their paper that higher infraction of nanoparticles volume along with a degeneration in the diameter of nanoparticle elevates the value of Nusselt number. Convection on micro along with nanoliquids with Cattaneo-Christov heat flux has been studied by [12]. Their flow equations are highly nonlinear and were solved via Runge-Kutta with shooting approach. It was finalized in

the paper that adding the nano uid rate of heat transport along with temperature distribution is much higher when compared to the micro uid. In a similar report, [13] in their study, reviewed the size of the particle's impact on nano uid viscosity.
Thermophoresis explains submicron-sized particles that migrate from one region to another. This particle requires a velocity called the thermophoretic velocity and the force is refers to as the thermophoretic force. The existence of mass plus heat transport together in a liquid that is on motion desires more investigations as the relationship that exist with the energy ux and the propelling potentials are more intricate than imagined. Dufour e ect is energy ux as a result of the composition slope. This e ect is found in the energy equation. Mass uxes that are created due to temperature gradient are referred to as the Soret contribution. This is found in the equation of concentration. [14], investigated Soret alongside Dufour impacts in their exploration. Their simpli ed ow model was solved via SRM. It was concluded in their exploration that an enhancement in the Dufour term degenerates velocity along with temperature pro les. [15], explored Soret together with Dufour impact on MHD heat couple with mass transport motion. Their result shows that the impact of Soret along with Dufour improves solutal boundary layer thickness. [16] considered in their study, Soret and Dufour contributions on MHD ow. Their motion model was solved numerically with the shooting approach. It was concluded in their study that Soret together with Dufour terms regulates heat alongside mass transport rate.
Mass and heat transport problems on non-Newtonian liquids has gained large interest in recent years. This is as a result of abundant applications in practical engineering processes. The performance of heat alongside mass transport transpiring at the same time in a moving uid results in complications between energy ux that are produced due to action between composition along with temperature gradients. The combined e ects of Soret along with Dufour in a uid can only occur when heat along with mass transport are examined together. [17] examined Soret along with Dufour e ect in stretching ow. The analytical approach was used and their ndings show that both Soret and Dufour have an improvement in temperature along with concentration. [18] recently elucidated on Soret along with Dufour mechanism on MHD heat together with mass transport by employing SHAM. In another reports, [19] obtained some results on the MHD motion of viscoelastic liquid with the heat source as well as thermal radiation using SHAM for their analysis. Their result revealed that heat source produces heat energy within the layers. [20] studied Soret-Dufour mechanism on an electrically conducting nano- uid with the in uence of buoyancy force, and chemical reaction while the combined in uence of soret and dufour has been examined on variable thermal conductivity and viscoelastic e ects on non-Newtonian uids through vertical porous plate by [21].
To the very best of my knowledge, no study in literature have considered the unsteady ow of both Casson and Walters-B uids simultaneously with Soret-Dufour mechanisms. Keeping this in mind, this study therefore explores the dynamics of non-Newtonian Casson-Walters-B nano uids ow past a semi-in nite vertical plate. The concentrated fruit juice and polymethyl methacrylate are the type of Casson and Walters-B uids examined in this study. These types of uids are very useful in industries where polymer are produced, and in industrial analysis to determine what uid and its appropriate properties is needed for the right application. Owing to this numerous applications, this study becomes very signi cant to both scientist and engineers. An iterative technique was employed on the system of equations. The signi cant e ects of ow parameters are depicted using graphs while quantities of engineering interest computations are presented with tables.

2. Equations of Motion

The problem of two-dimensional, laminar along with viscous electrically conducting Casson along with Walters-B liquid magneto-nanofluid motion past a vertical penetrable plate is considered in this paper. The surface temperature alongside concentration of the plate is assumed as $T_w > T_\infty$; $C_w > C_\infty$ where T_∞ and C_∞ are temperature along with concentration far from the boundary and T_w, C_w are wall temperature together with concentration (see Figure 1). The physical explanation of the flow of Casson alongside Walters-B phenomenon in a vertical penetrable plate is explored. The Walters-B and Casson liquid motion within the layers past the penetrable plate. The Casson liquid explored is blood while polymethyl methacrylate are the Walters-B liquid considered. The mixture of these fluids is noticeable at the boundary layer towards the hot region in the ambient vicinity. The quantity of Walters-B is lessens based on the wall and ambient difference in temperature (i.e. $T_w - T_\infty$). Magnetism of constant strength is assumed to oppose the fluids motion. The viscosity along with thermal conductivity is considered varied. We assumed Reynolds number of magnetic to be little so that induced magnetic is disregarded (see [20]). A homogeneous chemical reaction between fluid as well as species concentration is explored. In this paper, the approximation by Rosseland is employed in describing radiative heat flux because the fluid considered is optically thin. The present study is targeted on magneto-nanofluid flow which is an extension of the recent study of [20] to consider non-Newtonian fluids flow. The nanoparticles as seen in Figure 1 are assumed to possess magnetic characteristics situated in the hot region in the fluid layers.

The rheological analysis for Walters-B fluid can be illustrated as follows:

$$\tau_{ik} = -p g_{ik} + \tau'_{ik} \tag{2.1}$$

$$\tau'^{ik} = 2\eta_0 e^{ik} - 2k_0 e'^{ik} \tag{2.2}$$

here η_0 means rates of shear limiting viscosity, k_0 means co-efficient of elastic, τ^{ik} means stress tensor, p means isotropic pressure, g_{ik} means metric tensor of a static co-ordinate system x^i, v_i means velocity vector. The contravarient form of e'^{ik} is given by;

$$e'^{ik} = \frac{\partial e^{ik}}{\partial t} + v^m e^{ik}_{;m} - V^k_{;m} e^{im} - v^i_{;m} e^{mk} \tag{2.3}$$

The deformation rate tensor convected derivative is e^{ik} is

$$2e^{ik} = v_{i;k} + v_{k;i} \tag{2.4}$$

The limiting viscosity η_0 is defined as:

$$\eta_0 = \int_0^\infty N(\tau)\,d\tau \quad \text{and} \quad k_0 = \int_0^\infty \tau N(\tau)\,d\tau \tag{2.5}$$

$N(\tau)$ means relaxation spectrum as explored by (see [22]). This model is a valid analysis of Walters-B when short relaxation time is explained so that terms relating to

$$\int_0^\infty t^n N(\tau)\,d\tau \quad ; n \geq 2 \tag{2.6}$$

has been forgone and k_0 is taking to be significant. Also in [22], viscosity is defined as $\mu = \left.\frac{\partial u}{\partial y}\right|_{y=0}$ which means that Casson rheological analysis can be illustrated as:

(2.7)
$$\begin{cases} \tau_{ij} = \left(\mu_b(T) + \frac{P_y}{\sqrt{2\pi}}\right) 2e_{ij} & \text{when } \pi > \pi_c \\ \tau_{ij} = \left(\mu_b + \frac{P_y}{\sqrt{2\pi_c}}\right) 2e_{ij} & \text{when } \pi < \pi_c; \end{cases}$$

where P_y means yield stress of the Casson liquid expressed as

(2.8)
$$P_y = \frac{\mu_b \sqrt{(2\pi)}}{\beta}$$

μ_b means plastic viscosity, $\pi = e_{ij} e_{ij}$ means multiplication of deformation rate together and e_{ij} is the deformation rate and π_c is the critical value of Casson model analysis. The Casson flow where $\pi > \pi_c$, it is expedient to obtain

(2.9)
$$\nu_0 = \mu_b + \frac{P_y}{\sqrt{2\pi}}$$

invoking equation (2.8) into (2.9), the kinematic viscosity and plastic dynamic viscosity μ_b depends on each other while the density ρ and the Casson term β leads to

(2.10)
$$\nu_0 = \frac{\mu_b}{\rho}\left(1 + \frac{1}{\beta}\right)$$

Using the Boussinesq's approximation together with the assumptions above, the equations of motion are

(2.11)
$$\frac{\partial \bar{v}}{\partial \bar{y}} = 0$$

(2.12)
$$\begin{cases} \frac{\partial \bar{u}}{\partial \bar{t}} + \bar{v}\frac{\partial \bar{u}}{\partial \bar{y}} = \nu\left(1 + \frac{1}{\beta}\right)\frac{\partial^2 \bar{u}}{\partial \bar{y}^2} + g\beta_T(T - T_\infty) + g\beta_C(C - C_\infty) \\ \quad - \frac{\sigma B_0^2}{\rho}\bar{u} - \frac{\nu}{K}\left(1 + \frac{1}{\beta}\right)\bar{u} - \frac{K_0}{\rho}\left(\frac{\partial^3 \bar{u}}{\partial \bar{t}\partial \bar{y}^2} - \bar{v}\frac{\partial^3 \bar{u}}{\partial \bar{y}^3}\right) \end{cases}$$

(2.13)
$$\begin{cases} \frac{\partial T}{\partial \bar{t}} + \bar{v}\frac{\partial T}{\partial \bar{y}} = \alpha\frac{\partial^2 T}{\partial \bar{y}^2} - \frac{1}{\rho c_p}\frac{\partial q_r}{\partial \bar{y}} + \frac{\nu}{c_p}\left(1 + \frac{1}{\beta}\right)\left(\frac{\partial \bar{u}}{\partial \bar{y}}\right)^2 + \frac{Dk_T}{c_s c_p}\frac{\partial^2 C}{\partial \bar{y}^2} \\ \quad + \frac{Q_0}{\rho c_p}(T - T_\infty) + \tau_u\left[D_B\frac{\partial C}{\partial \bar{y}}\frac{\partial T}{\partial \bar{y}} + \frac{D_T}{T_\infty}\left(\frac{\partial T}{\partial \bar{y}}\right)^2\right] \end{cases}$$

(2.14)
$$\frac{\partial C}{\partial \bar{t}} + \bar{v}\frac{\partial C}{\partial \bar{y}} = D\frac{\partial^2 C}{\partial \bar{y}^2} - R(C - C_\infty) + \frac{Dk_T}{T_m}\frac{\partial^2 T}{\partial \bar{y}^2} + \frac{D_T}{T_\infty}\frac{\partial^2 T}{\partial \bar{y}^2}$$

Subject to

(2.15)
$$\bar{u} = u_0; \quad T = T_w + \varepsilon(T_w - T_\infty)e^{\bar{n}\bar{t}}; \quad C = C_w + \varepsilon(C_w - C_\infty)e^{\bar{n}\bar{t}} \quad \bar{y} = 0$$

(2.16)
$$\bar{u} \to 0; \quad T \to T_\infty; \quad C \to C_\infty; \quad \text{as } \bar{y} \to \infty$$

The integration of both sides of equation (2.11) gives constant which is the plate suction velocity. It is taken as a function of constant as well as time expressed in the published work of [14] as:

(2.17)
$$\bar{v} = -v_0(1 + \varepsilon A e^{\bar{n}\bar{t}})$$

Now employing the Rosseland approximation on the flow as reported by [5] such that

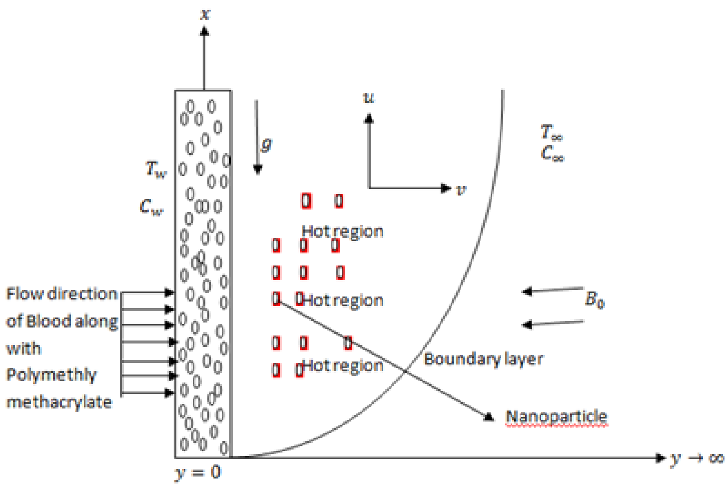

Figures 1: Flow Geometry

(2.18) $$q_r = -\frac{4\sigma_0}{3k_e}\frac{\partial T^4}{\partial y}$$

Since the present study uses the Rosseland approximation, hence the present paper is based on optically thin fluids. Assuming difference in temperature between the region of flow is insignificant such that Taylor's series expansion about T_∞ is used to expand T^4 in equation (2.18) and avoiding higher order term to obtain:

(2.19) $$T^4 = 4T_\infty^3 T - 3T_\infty^4$$

The model equations alongside boundary constraints are set into motion and written in a dimensionless by introducing

(2.20) $$U = \frac{\bar{u}}{u_0};\quad y = \frac{v_0^2 \bar{y}}{\nu};\quad t = \frac{v_0^2 \bar{t}}{\nu};\quad n = \frac{\bar{n}\nu}{v_0^2}$$

(2.21) $$\theta = \frac{T - T_\infty}{T_w - T_\infty};\quad \varphi = \frac{C - C_\infty}{C_w - C_\infty};$$

Applying eqns (2.17)-(2.21) on (2.11)-(2.14), we have the dimensionless form of equations

(2.22) $$\begin{cases} \frac{\partial U}{\partial t} - \left(1 + \varepsilon A e^{nt}\right)\frac{\partial U}{\partial y} = \left(1 + \frac{1}{\beta}\right)\frac{\partial^2 U}{\partial y^2} + \left(\lambda_a\theta + \lambda_b\varphi\right) \\ -\left(M + \frac{1}{Ps}\right)\left(1 + \frac{1}{\beta}\right)U + \gamma\frac{\partial^3 U}{\partial t\,\partial y^2} + \delta\frac{\partial^3 U}{\partial y^3} \end{cases}$$

(2.23) $$\begin{cases} \frac{\partial \theta}{\partial t} - \left(1 + \varepsilon A e^{nt}\right)\frac{\partial \theta}{\partial y} = \frac{1+Rd}{Pr}\frac{\partial^2 \theta}{\partial y^2} + Ec\left(1 + \frac{1}{\beta}\right)\left(\frac{\partial U}{\partial y}\right)^2 \\ + Du\frac{\partial^2 \varphi}{\partial y^2} + He\theta + Nb\frac{\partial \varphi}{\partial y}\frac{\partial \theta}{\partial y} + No\left(\frac{\partial \theta}{\partial y}\right)^2 \end{cases}$$

(2.24) $$\frac{\partial \varphi}{\partial t} - \left(1 + \varepsilon A e^{nt}\right)\frac{\partial \varphi}{\partial y} = \frac{1}{Sc}\frac{\partial^2 \varphi}{\partial y^2} - Cr\varphi + Sr\frac{\partial^2 \theta}{\partial y^2} + \frac{Nb}{LnNo}\frac{\partial^2 \theta}{\partial y^2}$$

along the boundary constraints

$$U = 1;\ \theta = 1 + \varepsilon e^{nt};\ \phi = 1 + \varepsilon e^{nt} \quad \text{at } y = 0 \tag{2.25}$$

$$u \to 0;\ \theta \to 0;\ \phi \to 0 \quad \text{at } y \to \infty \tag{2.26}$$

where the following are the parameters evolved in the present analysis and defined as follows:

$\bar{u}$-velocity in $\bar{x}$ direction (m/s), $\bar{v}$- velocity in $\bar{y}$ direction (m/s), $\bar{t}$-time (s), C- dimensional concentration (m^2/s), c_p-specific heat (J/kgK), D-mass diffusivity (m^2/s), g-gravity (m/s^2), R-chemical reaction term, / - thermal diffusivity of fluid(Kmolm^{-3}), - thermal expansion (K^{-1}), -concentration expansion (m^3/Kmol), - kinematic viscosity (m^2/s), - density (kg/m^3), k_T- thermal diffusion ratio, T_m-mean Fluid Temperature (K), T_∞ -ambient temperature (K), C_∞ -ambient concentration (mol), -Electrical conductivity , B_0-external imposed magnetism strength in y direction, q_r- heat flux (W/m^2), c_s-concentration susceptivity (Kmol/m^3), -viscosity (m^2/s), T- fluid temperature (K), $\bar{n}$-constant, D_B Brownian coefficient, Q_0 heat generation coefficient, $_u$ thermophoretic coefficient, T_w; C_w-wall temperature (K) and concentration (mol) respectively, $G_a = \frac{g\, v\,(T_w - T_\infty)}{u_0 v_0^2}$ mass Grashof number, $G_b = \frac{g\, v(C_w - C_\infty)}{u_0 v_0^2}$ thermal Grashof number, $M = \frac{B_0^2 v}{v_0^2 u_0}$ magnetic term, $D_u = \frac{D_m}{C_s}\frac{k_T}{c_p}\frac{(C_w - C_\infty)}{v(T_w - T_\infty)}$ Dufour number, $S_r = \frac{D_m K_T}{T_m}\frac{(T_w - T_\infty)}{(C_w - C_\infty)}$ Soret number, $E_c = \frac{{}_0^2}{c_p(T_w - T_\infty)}$ Eckert number, $N_o = \frac{D_B(C_w - C_\infty)}{}$ thermophoretic parameter, $N_b = \frac{D_T(T_w - T_\infty)}{T_\infty}$ Brownian motion parameter, $He = \frac{Q_0}{c_p u_0}$ Heat generation parameter, $Rd = \frac{4\,{}_0 T_\infty^3}{k_e k}$ Thermal radiation parameter, $Sc = \frac{}{D}$ Schmidt number, $Cr = \frac{R}{u_0}$ Chemical reaction parameter, $Ln = \frac{}{D_B}$ Lewis number, $Pr = -$ Prandtl number, $P_s = \frac{}{ku_0}$ Permeability parameter.

The quantities of physical interest are defined in this study as:

Local skin friction: $C_f = \frac{_w}{u_0 v_0}$;

Nusselt number: $Nu = \frac{Kq_w}{(T_w - T_\infty)}$;

Sherwood number: $Sh = \frac{D_m S_w}{(C_w - C_\infty)}$

where

$$_w = {}_0 \frac{\partial \bar{u}}{\partial \bar{y}}\Big|_{\bar{y}=0} \quad \frac{\partial^2 \bar{u}}{\partial \bar{t}\,\partial \bar{y}} + \frac{\partial^3 \bar{u}}{\partial \bar{y}^2}\Big|_{\bar{y}=0}$$

$$q_w = K \frac{\partial T}{\partial \bar{y}}\Big|_{\bar{y}=0} \quad \frac{4\,{}_0}{3k_e}\frac{\partial T^4}{\partial \bar{y}}\Big|_{\bar{y}=0}$$

$$S_w = \frac{\partial C}{\partial \bar{y}}\Big|_{\bar{y}=0}$$

3. Spectral Relaxation Techniques

This section gives a brief explanation of the spectral relaxation techniques (SRM). In applying SRM, the current iteration level is assumed to be evaluated at $(r + 1)$ while other terms such as linear as well as nonlinear are known at the previous iteration denoted by (r) (see [23]). The above description on SRM is the basic idea of Gauss-seidel approach decoupling used in systems of equation (see [24]). This paper uses the Chebyshev spectral collocation methods to discretize the differential equations. Spectral methods are recognized for their high accuracy, ease implementation as well as smooth outcomes over simple domains. To apply the spectral methods, the domain of flow equations is transformed to a close interval $[\ 1;1]$. It is on this transformed domain we can solve the problem. The transformation $\ = \frac{L(\ +1)}{2}$ is used to map the interval $[0;L]$ to $[\ 1;1]$ where L is the scalling parameter approximated its conditions at infinity. As a result of the SRM scheme procedure described above, equations (2.22)-(2.24) becomes

$$[1+\ D^{2}]\frac{dU_{r+1}}{dt}=\frac{d^2U_{r+1}}{dy^2}+a_{0;r}\frac{dU_{r+1}}{dy}\quad a_{2;r}U_{r+1}+a_{3;r}\frac{d^3U_{r+1}}{dy^3}+a_{1;r} \tag{3.1}$$

$$\left(\begin{aligned} &Pr\frac{d\theta_{r+1}}{dt}=b_{0;r}\frac{d^2\theta_{r+1}}{dy^2}+b_{1;r}\frac{d\theta_{r+1}}{dy}+PrHg\theta_{r+1}\\ &\qquad +b_{4;r}\frac{d\theta_{r+1}}{dy}+b_{2;r}+b_{3;r}+b_{5;r}\end{aligned}\right. \tag{3.2}$$

$$Sc\frac{d\phi_{r+1}}{dt}=\frac{d^2\phi_{r+1}}{dy^2}+c_{0;r}\frac{d\phi}{dy}\quad ScCr\phi_{r+1}+c_{1;r} \tag{3.3}$$

Subject to:

$$U_{r+1}(0;t)=1;\ \ \theta_{r+1}=1+\ \ e^{nt};\ \ \phi_{r+1}=1+\ \ e^{nt}; \tag{3.4}$$

$$u_{r+1}(8;t)=0;\ \ \theta_{r+1}(8;t)=0;\ \ \phi_{r+1}(8;t)=0 \tag{3.5}$$

It should be noted that $a_{0;r}=\ \ 1+\ Ae^{nt}$; $a_{1;r}=\ _a\theta+\ _b\phi$; $a_{2;r}=\ \ M+\frac{1}{Ps}\ \ 1+\frac{1}{}$; $a_{3;r}=$; $b_{0;r}=1+Rd$; $b_{1;r}=Pr\ \ 1+\ Ae^{nt}$; $b_{2;r}=\ Ec\ \ 1+\frac{1}{}\ \ \frac{\partial U}{\partial y}^{2}$; $b_{3;r}=Pr\,Du\frac{\partial^2\phi}{\partial y^2}$; $b_{4;r}=Nb\frac{\partial\phi}{\partial y}$; $b_{5;r}=Pr\,No\ \frac{\partial\theta}{\partial y}^{2}$; $c_{0;r}=Sc\ \ 1+\ Ae^{nt}$; $c_{1;r}=Sr\frac{\partial^2\theta}{\partial y^2}+\frac{Nb}{LnNo}\frac{\partial^2\theta}{\partial y^2}$.

Following [25], the Gauss-Lobatto collocation points is used to define the nodes in $[\ 1;1]$ as

$$Y_j=\cos\ \frac{\ j}{Nx}\ \ ;\ \ j=0;1;:::;Nx \tag{3.6}$$

Difference scheme centering about a midpoint between t^{n+1} and t^n is employed on the iteration schemes (3.1)-(3.3). The centering about $t^{n+\frac{1}{2}}$ to any of the unknown function, say $u(y;t)$ and its associated derivative leads to

$$U(y_j;t^{n+\frac{1}{2}})=U_j^{n+\frac{1}{2}}=\frac{U_j^{n+1}+U_j^n}{2};\qquad \frac{\partial U}{\partial t}^{n+\frac{1}{2}}=\frac{U_j^{n+1}\quad U_j^n}{\Delta t} \tag{3.7}$$

$$\theta(y_j;t^{n+\frac{1}{2}})=\theta_j^{n+\frac{1}{2}}=\frac{\theta_j^{n+1}+\theta_j^n}{2};\qquad \frac{\partial\theta}{\partial t}^{n+\frac{1}{2}}=\frac{\theta_j^{n+1}\quad \theta_j^n}{\Delta t} \tag{3.8}$$

$$\phi(y_j;t^{n+\frac{1}{2}})=\phi_j^{n+\frac{1}{2}}=\frac{\phi_j^{n+1}+\ _j^n}{2};\qquad \frac{\partial\phi}{\partial t}^{n+\frac{1}{2}}=\frac{\phi_j^{n+1}\quad \phi_j^n}{\Delta t} \tag{3.9}$$

Applying the procedure of spectral method on (3.1)-(3.3) first before the implementation of finite difference method to give

(3.10) $$[1 + \ D^{2}]\frac{dU_{r+1}}{dt} = (\ D^{2} + a_{0;r}D + a_{3;r}D^{3} \quad a_{2;r})U_{r+1} + a_{1;r}$$

(3.11) $$Pr\frac{d\#_{r+1}}{dt} = (\ b_{0;r}D^{2} + b_{1;r}D + PrHg + b_{4;r}D)\#_{r+1} + b_{2;r} + b_{3;r} + b_{5;r}$$

(3.12) $$Sc\frac{d'_{\ r+1}}{dt} = (\ D^{2} + c_{0;r}D \quad ScCr)'_{\ r+1} + c_{1;r}$$

subject to (3.4) and (3.5) where
We now proceed to apply the nite di erence sceme on equations (3.10)-(3.12) in direction of t and de ned mid-point $t^{n+\frac{1}{2}}$ to yield

(3.13) $${}_{1}U_{r+1}^{n+1} = \ {}_{2}U_{r+1}^{n} + K_{1}$$

(3.14) $${}_{3}\#_{r+1}^{n+1} = \ {}_{4}\#_{r+1}^{n} + K_{2}$$

(3.15) $${}_{5}'^{\ n+1}_{\ r+1} = \ {}_{6}'^{\ n}_{\ r+1} + K_{3}$$

Subject to

(3.16) $$U_{r+1}(xNx; t^{n}) = \#_{r+1}(xNx; t^{n}) = '_{\ r+1}(xNx; t^{n}) = 0$$

(3.17) $$U_{r+1}(x_{0}; t^{n}) = 1;\ \ \#_{r+1}(x_{0}; t^{n}) = 1 + \ e^{nt};\ \ '_{\ r+1}(x_{0}; t^{n}) = 1 + \ e^{nt}$$

where

$${}_{1} = \frac{(1 + \ D^{2})}{4\ t} \quad \frac{(D^{2} + a_{0;r}D + a_{3;r}D^{3} \quad a_{2;r})}{2};$$

$${}_{2} = \frac{(1 + \ D^{2})}{4\ t} + \frac{(D^{2} + a_{0;r}D + a_{3;r}D^{3} \quad a_{2;r})}{2};$$

$${}_{3} = \frac{Pr}{\ t} \quad \frac{(b_{0;r}D^{2} + b_{1;r}D + b_{4;r}D + PrHg)}{2};$$

$${}_{4} = \frac{Pr}{4\ t} + \frac{(b_{0;r}D^{2} + b_{1;r}D + b_{4;r}D + PrHg)}{2};$$

$${}_{5} = \frac{Sc}{4\ t} \quad \frac{(D^{2} + c_{0;r}D \quad ScR_{c})}{2}; \qquad {}_{6} = \frac{Sc}{4\ t} + \frac{(D^{2} + c_{0;r}D \quad ScR_{c})}{2};$$

and

$$K_{1} = a_{1;r}^{n+\frac{1}{2}};\quad K_{2} = (\ b_{2;r}^{n+\frac{1}{2}} + b_{3;r}^{n+\frac{1}{2}} + b_{5;r}^{n+\frac{1}{2}});\quad K_{3} = c_{1;r}^{n+\frac{1}{2}}$$

4. Results along with Discussion

The numerical results obtained from solutions of the coupled third order PDE (2.22)-(2.24) employing SRM is discussed. The numerical computations is coded in MATLAB program. The contribution of key parameters on velocity, concentration as well as temperature pro les is extensively discussed. To be realistic with the obtained results, we have chosen the Prandtl number (Pr) to be 0:71 which represents air at 25^0C and the Schmidt numeric (Sc) chosen for hydrogen i.e 0:22, water vapor i.e 0:62, ammonia i.e 0:78 and carbon-dioxide i.e 0:94 at 25^0C while values of other ow parameters are; $= 3{:}0$; $_a =$ $_b = 2{:}0$; $M = 1$; $Ps = 0{:}4$; $= 0{:}2$; $Rd = He = 0{:}5$; $Ec = 0{:}01$; $Du = 3{:}0$; $Nb = 0{:}7$; $No = 0{:}9$; $Cr = 0{:}6$; $Sr = 2{:}5$; $Ln = 0{:}3$; $= 0{:}001$; $A = 0{:}5$; $n = 1$. All the parameters were chosen based on experimental computations. Also noting that $Gr > 0$ corresponds to cooling of the plate.

4.1. Velocity Pro les.

The contributions are as stated below:

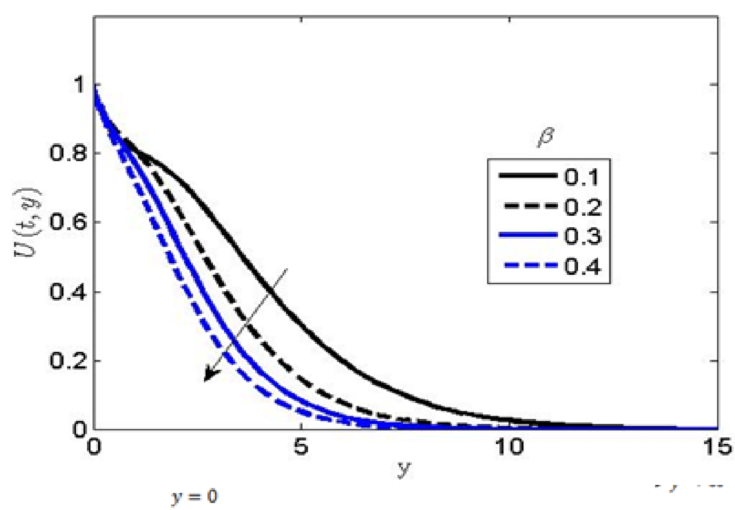

Figures 2a: Contribution of Casson parameter ( ) on the velocity plot

Figure 2(a) represent the contribution of Casson parameter ( ) on velocity pro le. Increasing the numeric value of is detected to degenerate the velocity plot. Starting from the initial point to the boundary (1 = y = 8), a gradual degeneration of velocity along with the entire hydrodynamic boundary layer is detected. The dynamic plastic viscosity possess by the Casson uid becomes very high as the value of is increased coupled with the hot region. Because of the hot region, the blood becomes very light and as heat is generated due to heat source and the hot region. This experiment shows that this e ects degenerates the velocity of the uid layer.

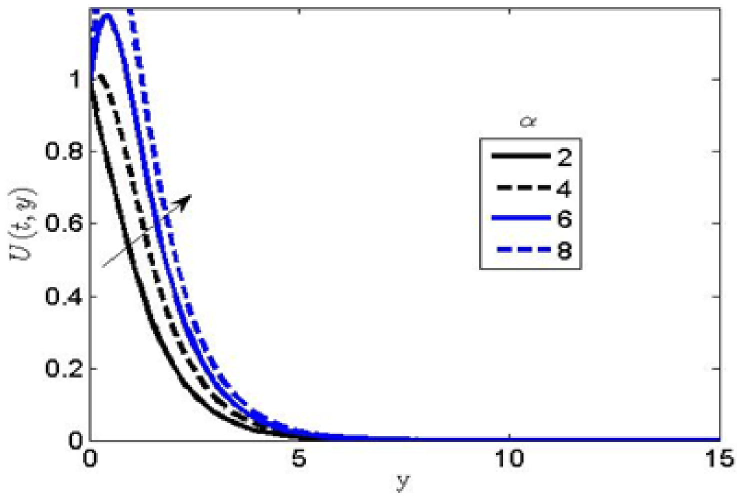

Figures 2b: Contribution of Walters-B liquid term ( ) on the velocity plot

Figure 2(b) explains the impact of Walters-B liquid term ( ) on velocity pro le. Higher value of is seen to enhance the uid velocity pro le. The increase that is experienced due to increase in is associated with the hot region within the boundary layer. The methyl methacrylate type of Walters-B liquid considered in the present study belongs to antigen group which is capable of inducing cellular immune reaction. This characteristics coupled with the hot region shown in Figure 1 along with the ow of methyl methacrylate with Casson uid (blood) is detected in Figure 2(b) to enhance velocity pro le close to the plate and has its strength gradually degenerating as it is approaching free stream(i:e ! 1).

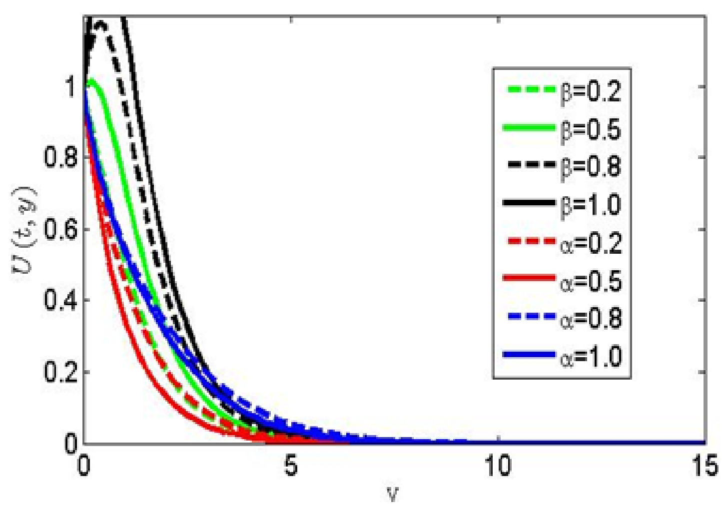

Figures 3a: Behavior of together with on velocity pro le

Figure 3(a) explains the simultaneous ow of blood and methyl methacrylate with the ow layers (i:e 1 y 1). The ow of blood is observed to be eractic closed to the wall compared with methyl methacrylate. This is noted to be as a result of constant dynamic plastic viscosity considered in this study.

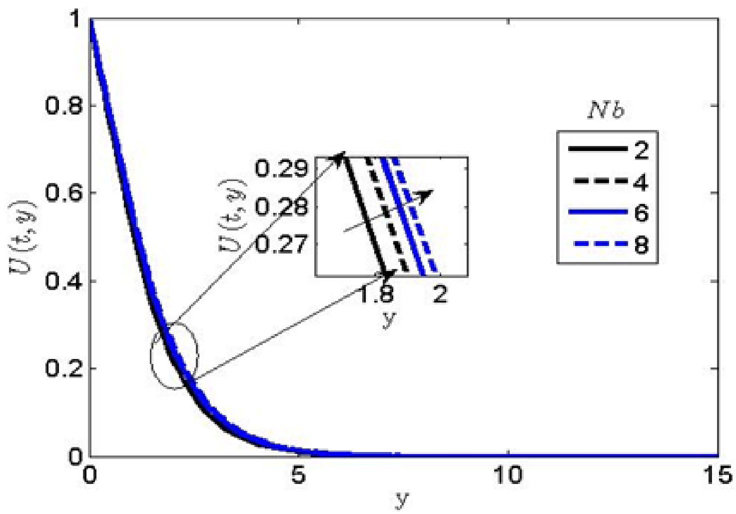

Figures 3b: Contribution of Nb on the velocity plot

Figure 3(b) represent the contribution of Brownian motion (Nb) on velocity pro le. E ect of Nb on velocity is noticed to be negligible close to the wall.Nb in uence on velocity is noticed . This is true owing to the region where impact ofNb is noticeable is hot. Hence, it is expected to enhance the thickness of the boundary layer.

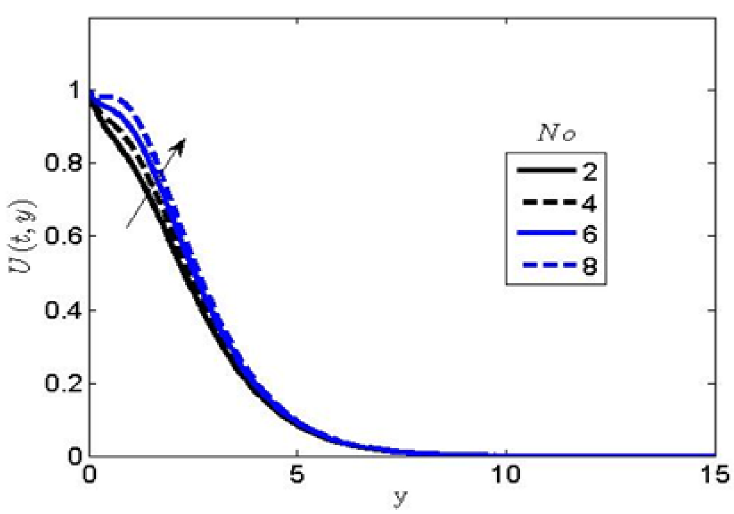

Figures 4a: E ect of No on velocity plot

The in uence of thermophoretic term (No) on velocity plot with viscous dissipation is shown in Figure 6. Thermophoresis portray the migration of small particles from a cold region to hot region. The presence of viscous dissipation along with the hot region as shown in Figure 1, thereby heat up the boundary layer more and produces a kinetic energy which helps the non-Newtonian uids couple with nanoparticles within the layer. It is observed that No a ect velocity and temperature plot.

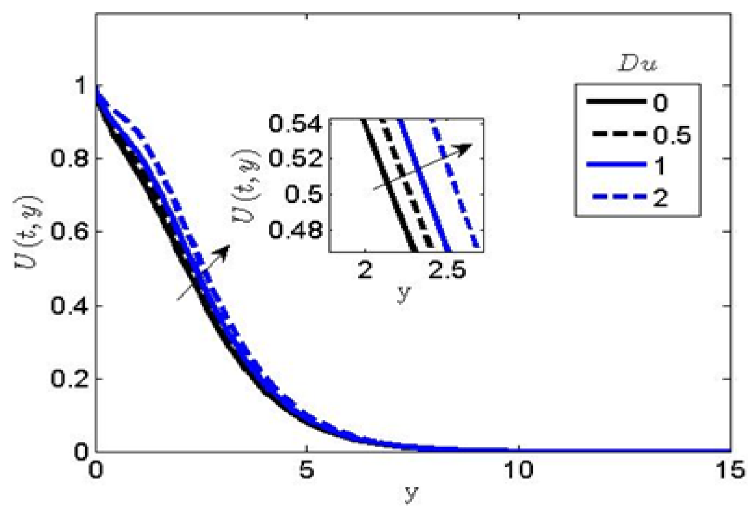

Figures 4b: Contribution of Du on velocity plot

The impact of Dufour (Du) on velocity plot is given in Figure 4(b). Our experiment shows that increasingDu lead to enhancement of both velocity pro les. This is expected in the analysis of heat along with mass transfer. The particles di uses spontaneously as the value of Dufour number increases to enhance the thermal layer thickness.

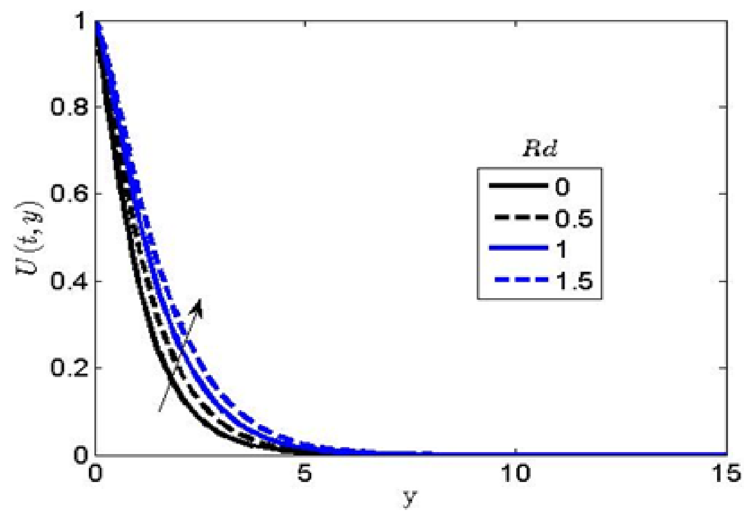

Figures 5a: Contribution of thermal radiation on velocity plot

Figure 5(a) present the contribution of radiation term (Rd) on velocity plot. Increasing thermal radiation parameter (Rd) means a strong rise in radiative heat that is loss because of ambient temperature along with velocity. Because of this heat energy is release by the uid to ow region and results to cooling of the structure. As depicted in gure 5(a), increase in Rd produces a signi cant upsurge in velocity. The ow domain is within 0 y 15. Within this domain there is hot region as shown in gure 1. As Rd increases, it leads to more heat at this region within the uid layers. The blood and polymethly methacrylate ows into the hot region past the vertical penetrable plate. On getting to this region in the ow domain, they mixed together and both uids becomes lighter and posses less viscosity. In view of this, they moved faster in the boundary layer with a ow distance 0 y 15 Their fast movement is owing to increasing values of thermal radiation term which brings increase to momentum. This experiment again shows that thermal radiation has great impact on the motion regime. Hence, the study shows that the contribution of radiation becomes very useful as $Rd \neq 0$ and $Rd \to 1$:

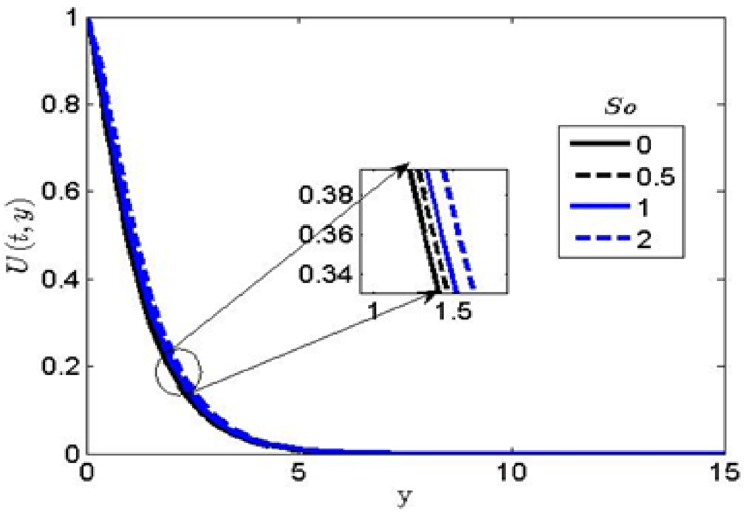

Figures 5b: Contribution of Soret number on velocity plot

The impact of Soret term (So) on velocity is represented in Figure 5(b). The Soret term is found to elevate velocity. This experiment indicates that (So) is responsible for thermal di usion within the boundary layer. As this helps the uids to di use evenly in the layers, the uid strength and momentum suddenly rise with the concentration of the uid.

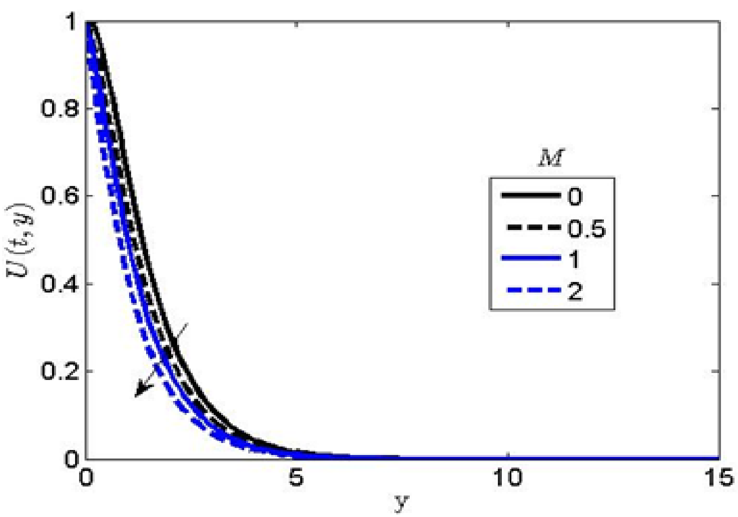

Figures 6a: Contribution of magnetic term on the velocity plot

The impact of magnetic eld term (M) on velocity plot is represented in Figure 6(a). It is found out from Figure 6(a) that (M) degenerate the uid velocity because of the imposed transversed magnetic eld to generate Lorentz drag force. This force is responsible for slowing down transport of electrically as well as conducting liquid within the boundary layer. The Lorentz force is responsible for degeneration of uid velocity strating from the hot region close to the plate immediately magnetic eld opposes the heat together with mass transport phenomena. Because of this drag-like force generated by the in icted magnetism and increase in M the more, deceleration of velocity of velocity is noticed in Figure 6(a). This study equally a rmed that, the Lorentz force produced generate friction which reduces the heat energy but the hot region at the layers reduces the uid strength. Blood and polymethly methacrylate mixed and get contaminated with the nano uid at the hot region. Thus the velocity layer thickness along with the velocity decreases.

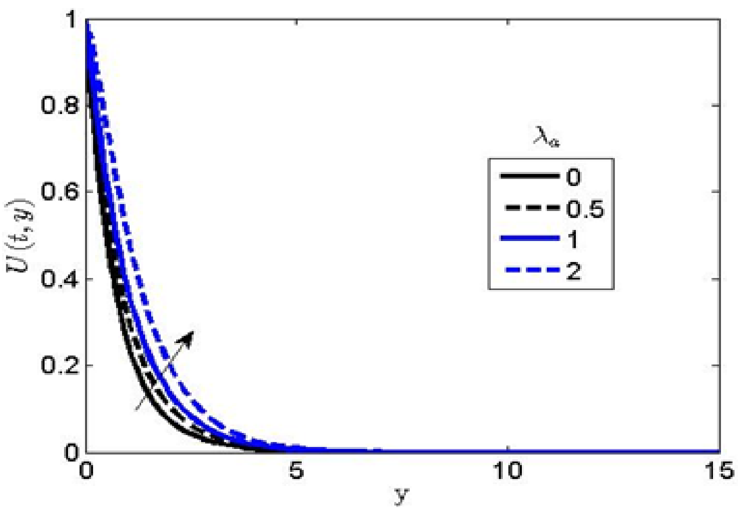

Figures 6b: E ect of thermal Grashof number on velocity pro les

Figure 6(b) portray the contribution of thermal Grashof number ($_a$) on velocity pro le. Increasing $_a$ helps to boost velocity for the case $Pr = 0{:}71$ that is for air. The velocity overshoot within the layer region because force of buoyancy acts like a pressure gradient and elevates the uids within the layers.

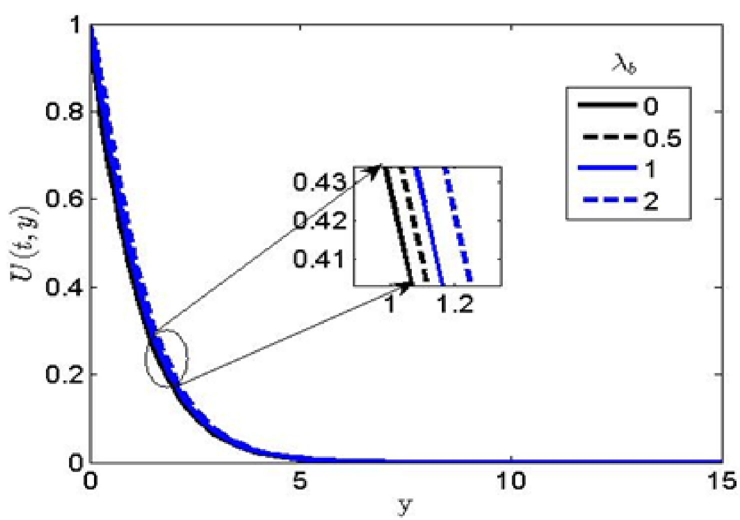

Figures 7a: E ect of mass Grashof number on velocity pro le

Figure 7(a) described the impact of mass Grashof number ($_a$) on velocity pro le. Increasing $_b$ helps to boost velocity for the case $Pr = 0{:}71$ that is for air. The velocity overshoot within the layer region because force of buoyancy behaves like a pressure gradient and elevates the uids within the layers. This behavior is very similar to that experienced with thermal Grashof number e ects.

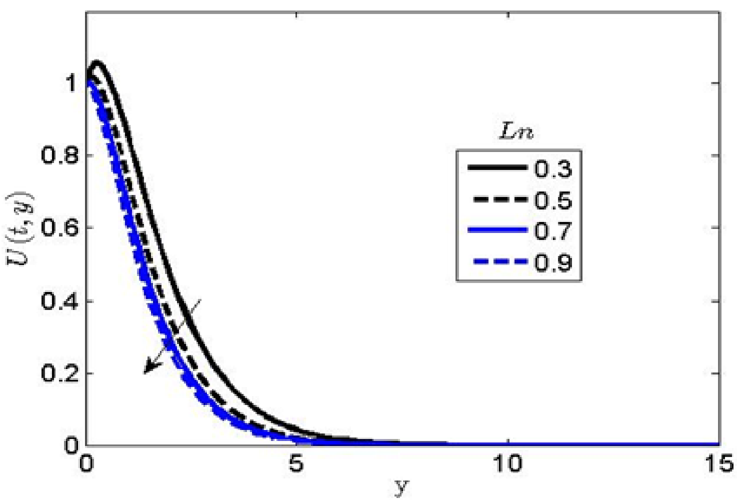

Figures 7b: E ect of Lewis number on velocity pro le

The e ect of Lewis number (Ln) on velocity pro le is illustrated in Figure 7(b). It is noticed that large value of Ln results to reduction in velocity pro le. Ln depict the quotient of thermal conductivity to mass di usivity. Physically, large thermal conductivity along with lower mass di usivity results to higher Lewis number and vice versa. However, increasing the Lewis number means the imposition of much thermal conductivity than the mass di usivity. High values of Ln is equivalent to weaker molecular di usivity alongside thinner layer thickness.

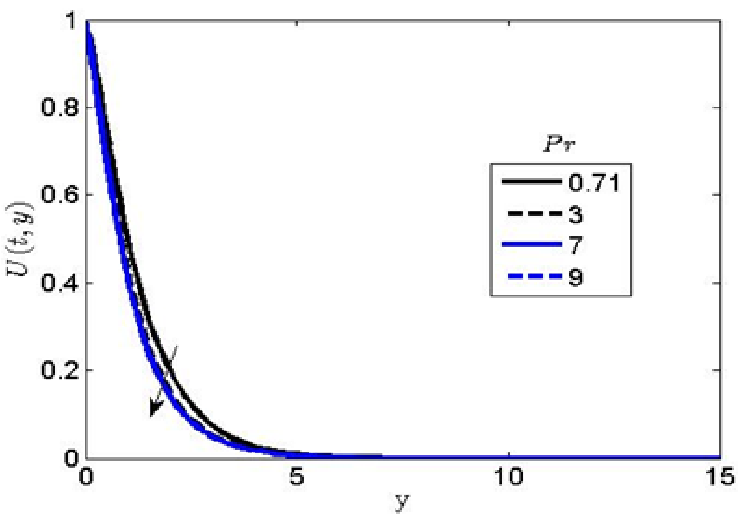

Figures 8a: Contribution of Prandtl term on velocity pro le

Figure 8(a) depicts the contribution of Prandtl number (Pr) on velocity plot. It is observed from Figure 8a that velocity along with temperature for $Pr = 0:71$ is higher than $Pr = 3$ and 7. Pr described the quotient of uid viscosity to thermal conductivity. This physically indicates that higher viscosity leads to much Prandtl number. The results in Figure 8(a) is possible because high Pr corresponds to high viscosity and hence uids in the layers moves slowly. This is because there is degeneration in thermal layer thickness by reducing the average temperature within the boudnary layer. Greater Pr plays a predominat role in controlling both thermal di usivity and momentum di usivity in the analysis of heat together with mass transport.

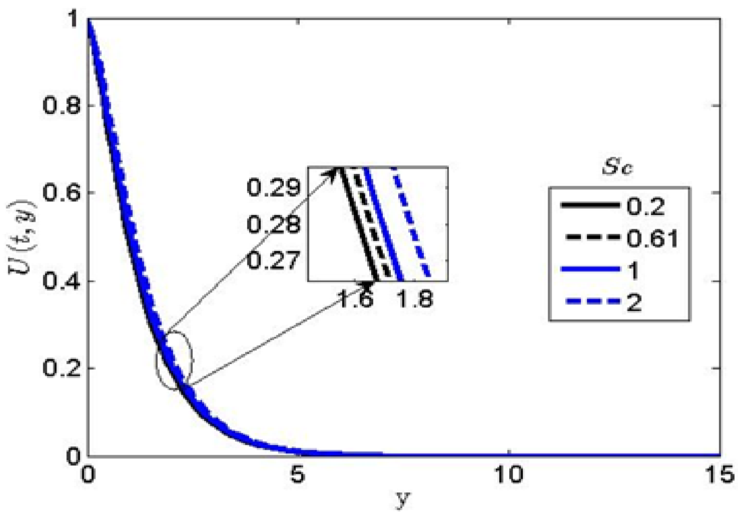

Figures 8b: E ect of Schmidt number on velocity pro le

The impact of Schmidt number (Sc) on velocity plot is illustrated in Figure 8(b). The Schmidt number is de ned as the quotient of uid viscosity against mass di usivity. This indicate that high viscosity leads to high Sc with the boundary layer. Higher uid velocity is because of the fact that mass di uses greatly in the boundary layer with lower uid. The Schmidt number Sc is given as $\frac{}{D}$. To be realistic in this study, the values of Sc at room temperature 25^0C and 1 atmospheric pressure were used, while for hydrogen ($Sc = 0:22$) and water vapor ($Sc = 0:6$).

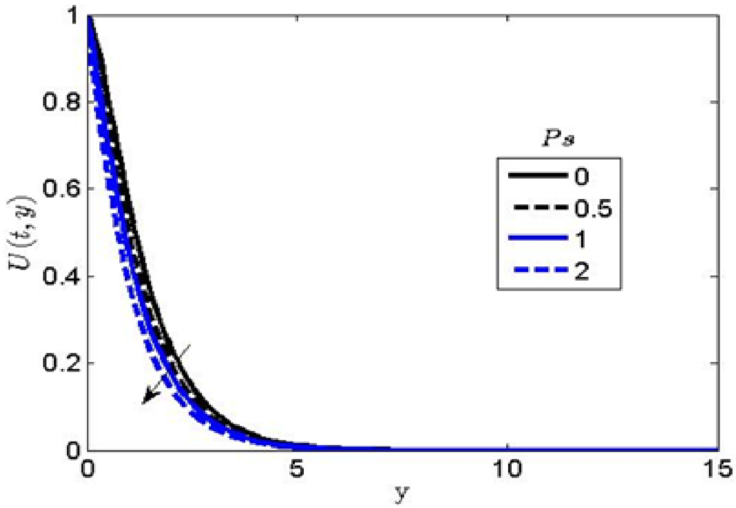

Figures 9a: E ect of porosity term on velocity pro le

Figure 9(a) portray the in uence of permeability term (Ps) on velocity plot. Ps is seen to reduce the velocity within the layer. Increase in the permeability parameter (Ps) reduces the velocity eld. Physically, increasing Ps gives more room to the motion of uid to the boundary layer. The more the porosity implies the lower the uid intensity within the layer. Increasing the value of permeability term (Ps) simultaneously reduces the uid velocity and thickening of the thermal layer increases.

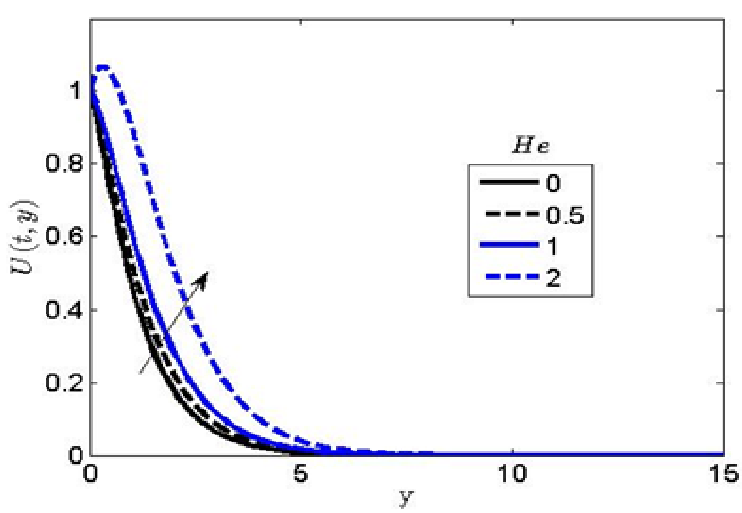

Figures 9b: Impact of heat generation on velocity plot

The in uence of heat generation term (He) on velocity plot is exhibited in Figure 9(b). Physically, when heat is generated the uid environment thermal condition becomes hot and because the boudary layer as shown in Figure 1 is hot, hence there is too much hotness within the layers. This automatically enhances the ow within the layer region.

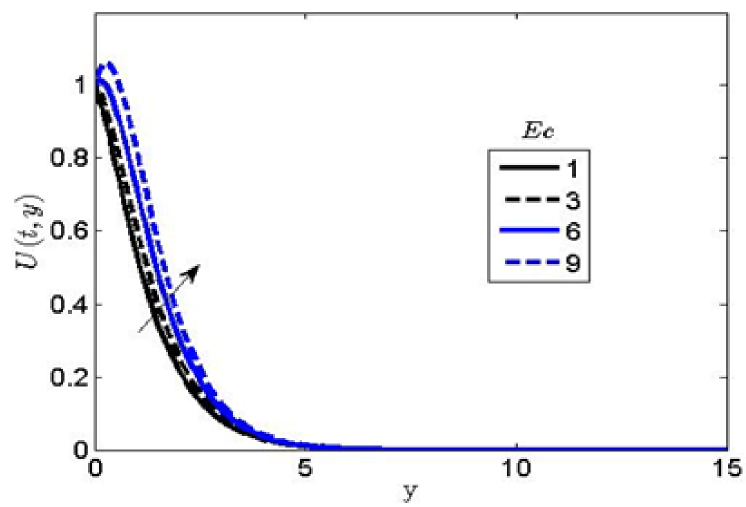

Figures 10: Contribution of Eckert number on velocity plot

The in uence of viscous dissipative term, that is, (Eckert number) on velocity plot is illustrated in Figure 10. Increasing Ec is seen to elevate the velocity plot respectively. The dissipative term responsible for transforming kinetic energy to internal energy which means heating up the uid. This is an irreversible process. Larger dissipation releases more heat and it will raise the temperature of the uid. The viscous dissipative term plays a signi cant role in uid ow with high viscosities.

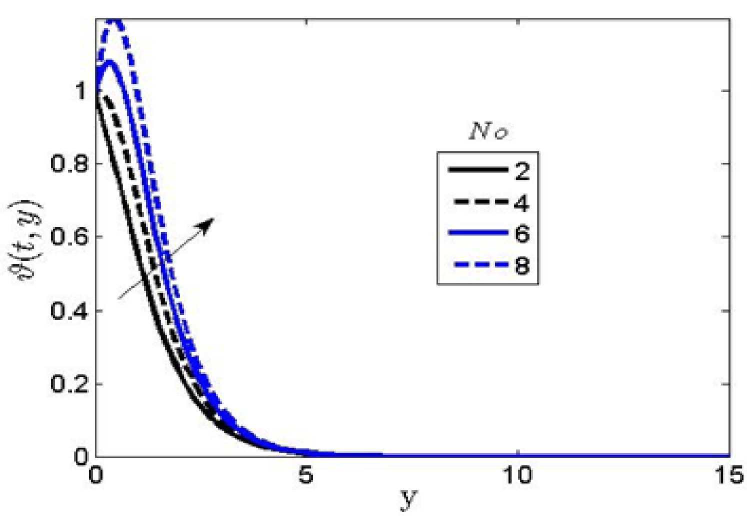

Figures 11a: E ect of thermophoretic parameter on temperature plot

The contribution of thermophoretic parameter (No) on temperature plot is shown in Figure 11(a). It is observed that No a ect the temperature pro le by producing a drastic upsurge. Increasing thermophoretic parameter with heat generation and the hot region in the boundary layer gives rise to heat energy and thereby increases the temperature alongside thermal boundary layer thickness.

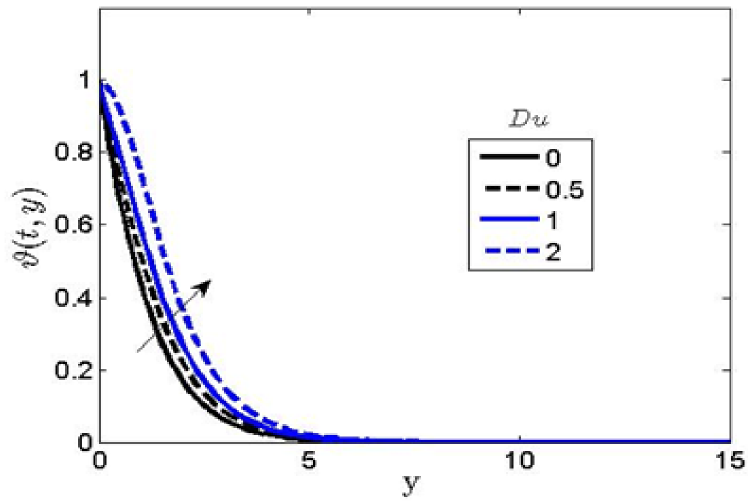

Figures 11b: Contribution of Dufour number on temperature plot

The contribution of Dufour (Du) on temperature pro le is depicted in Figure 11(b). Here, the numerical experiment shows that by increasing Du lead to enhancement of temperature pro les. This is expected because increasing the Dufour numbers helps the nanoparticles to di uses faster within the boundary layer due to more heat. Hence, the temperature along with the boundary layer thickness increases.

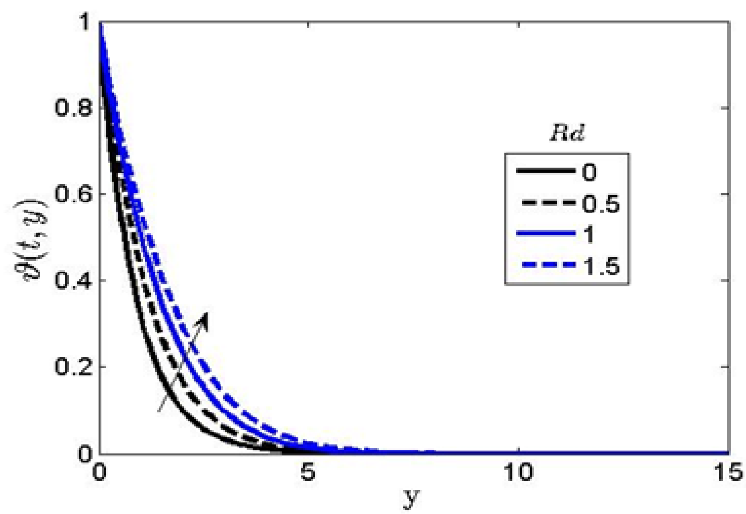

Figures 12a: Contribution of thermal radiation on temperature pro le

Figure 12(a) present the in uence of radiation term (Rd) on temperature pro le. Temperature pro le as seen in Figure 12(a) drastically increases because blood along with polymethly methacrylate considered in this study gets hotter as Rd increases coupled with the hot region to increase temperature along with thermal boundary layers. The study shows that thermal radiation has great impact on the motion regime. Hence, this experiment again shows that contribution of radiation is signi cant as $Rd \neq 0$ and $Rd \to 1$: The numerical calculations also show that thermal radiation increases alongside heat generation parameter. This phenomenon of hot region within the uid boundary layer is useful in convective flow. The thermal condition of the liquid also enhances, the moment thermal radiation increases.

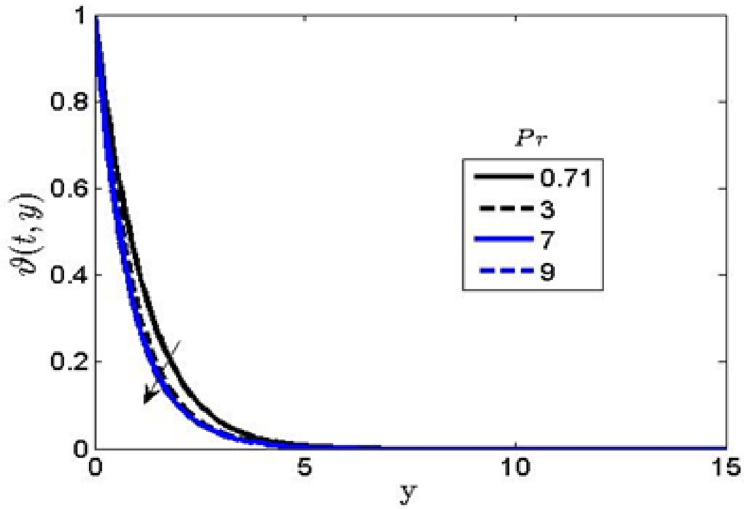

Figures 12b: Contribution of Prandtl number on temperature profile

Figure 12(b) depicts the contribution of Prandtl number (Pr) on temperature profile. Greater Pr plays a predominat role in controlling both thermal diffusivity and momentum diffusivity in the analysis of heat together with mass transport. Consider the value of $Pr = 0{:}71; 1; 3$ is related to air, electrolyte solution like salt water solution. Large value of Pr leads to less thermal conductivity. However Pr can be use to ride cooling rate in an electrically conducting fluids. In this exploration, there exists a temperature T_w at the wall and the temperature T_1 at the free stream which upsurge ($T_w \quad T_1$) and thermal layer thickness. We critically examined two things in the present study namely; (2.1) the removal of heat at the wall with the use of Fouriers law of conduction; (2.2) the behaviour of fluid particles at the boundary. The moment heat is removed at the wall, the fluids have access to the boundary layer which has a hot region. The thermal conductivity at the layer keeps declining due to excess of heat and thereby decreases the temperature along with the thermal boundary layer.

The contribution of viscous dissipative term, that is, (Eckert number) on temperature profile is given in Figure 13(a). Larger dissipation releases more heat and it will raise the temperature of the fluid. The viscous dissipative term plays a significant role in fluid flow with high viscosities. As a result of this, the fluid temperature and increases. This is because viscous dissipation impact on heat along with mass transport flow is to bring an upsurge to internal energy which lead to a greater fluid temperature and buoyancy force.

The contribution of heat generation term (He) on the temperature plot is exhibited in Figure 13(b). The use of Rosseland approximation in this study helps to boost the temperature of the fluid which results to enhancement in the thermal layer thickness. Hence, increasing He is found to drastically upsurge in the temperature plot as displayed in Figure 13(b). Immediately the mixture of blood and methyl methacrylate gets to the boundary layer flow regime where there is hot region.

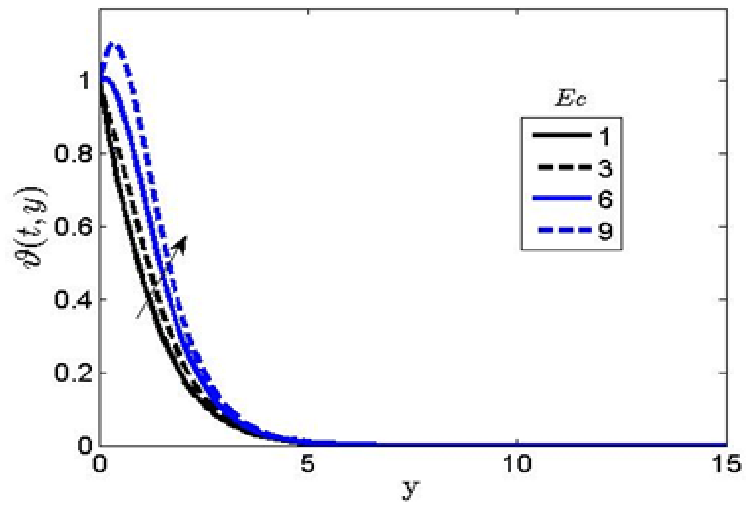

Figures 13a: E ect of Eckert number on temperature plot

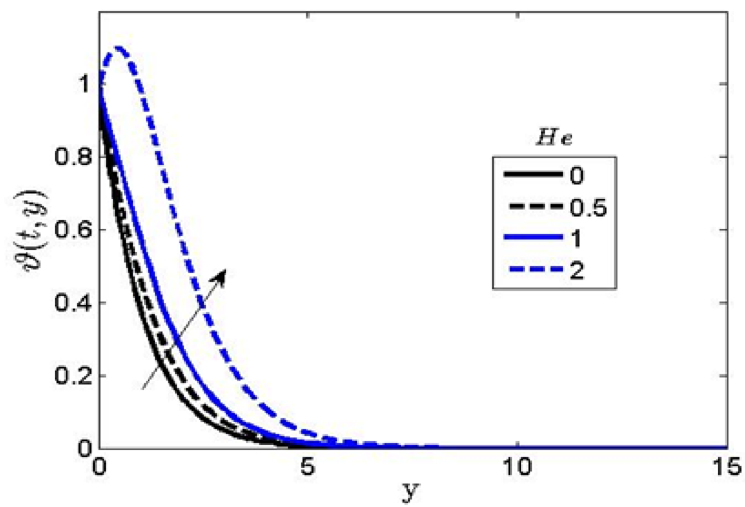

Figures 13b: Impact of heat generation on temperature plot

4.2. Concentration Pro les. Some impact are as follows:
Figure 14 represent the impact of Brownian motion (Nb) on temperature plot. E ect of Nb concentration pro le is noticed to be negligible near the wall but increases at the boundary layer. Nb in uences concentration far away from the plate. This is correct because at this region where impact of Nb is noticeable is hot. Hence, it is expected to enhance the thickness of the boundary layer.
The impact of Soret term (So) on concentration plot is displayed in Figure 15(a). The Soret term is found to elevate velocity along with concentration. Our experiment shows that So is responsible for thermal di usion within the boundary layer. As it helps the uids to di use evenly in the layers, the uid strength and momentum suddenly rise with the concentration of the uid.

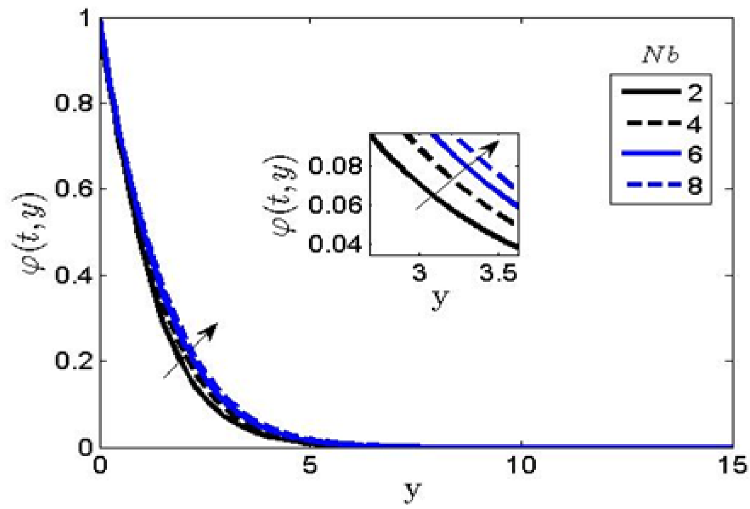

Figures 14: E ect of Brownian motion on the concentration plot

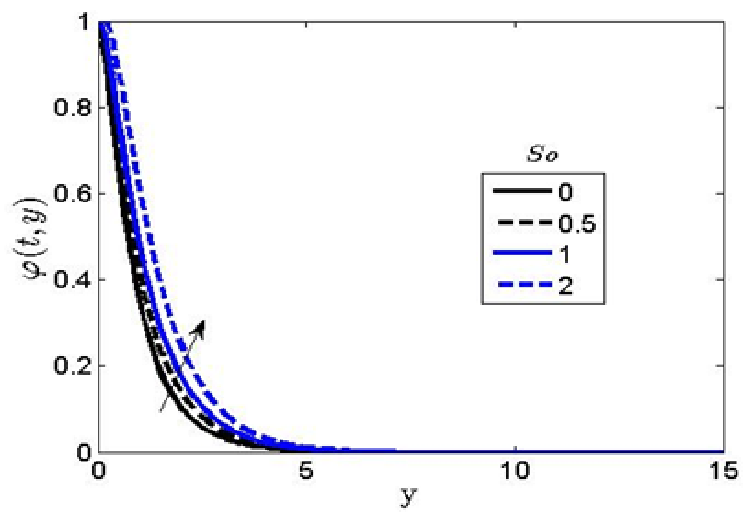

Figures 15a: Contribution of Soret number on concentration plot

The contribution of Lewis number (Ln) on concentration plot is illustrated in Figure 15(b). It is noticed that large value of Ln results to reduction in concentration pro le. Ln depict the quotient of thermal conductivity to mass di usivity. Physically, large thermal conductivity along with lower mass di usivity results to higher Lewis number and vice versa. However, increasing the Lewis number means the imposition of much thermal conductivity than the mass di usivity. High values of Ln is equivalent to weaker molecular di usivity alongside thinner layer thickness.
The impact of Schmidt number (Sc) on concentration plot is illustrated in Figure 16(a). This a ects the concentration buoyancy e ects and results to the acceleration of the velocity along with hydrodynamic the boundary layer region. Increase in the uid velocity is because of the fact that mass di uses greatly in the boundary layer with lower uid. The Schmidt number Sc is given as $\frac{}{D}$. In reality the values used for Sc at room temperature are 25^0C and 1 atmospheric pressure respectively, while for hydrogen is $Sc = 0{:}22$ and

Figures 15b: Contribution of Lewis number on concentration plot

Figures 16a: E ect of Schmidt number on concentration plot

water vapor is $Sc = 0{:}6$. It is noticed in Figure 16a that increase in Sc leads to degenerate temperature, concentration along with velocity distributions. From this experiment, it shows that, increasing Schmidt number lead to increase in the variable kinematic viscosity which brings decrease to the uid velocity. Base on the de nition of both Sc and Pr (i:e $Sc = \frac{\ }{D}$ $Pr = \frac{c_p}{k}$), the in uence of Sc on uid temperature is opposite in uence of Pr.

Figure 16(b) exhibit the impact of chemical reaction term (Cr) on concentration plot. The concentration boundary layer gets thinner as the chemical reaction increases. The study experiment shows that increasing the value of chemical reaction parameter leads to a destructive chemical reaction which degenerates the uid concentration as well as the solutal boundary layer thicknes.

Table 1: Validation of the present outcomes with published work of [26].